Evaluation of the Zn-O Complex and Oxygen-Donor Electron-Capture Cross Sections in p-Type GaP: Limits on the Quantum Efficiency of Red-Emitting (Zn,O)-Doped Material

J. S. Jayson, R. Z. Bachrach, P. D. Dapkus, and N. E. Schumaker

Bell Telephone Laboratories, Murray Hill, New Jersey 07974

(Received 23 March 1972)

The oxygen donor has been studied in a series of (Zn, O)-doped GaP samples. The infrared-luminescence intensity associated with this center was monitored over six decades of above band-gap photoexcitation intensity. A central feature of these measurements is a sublinear luminescent increase which extends over three decades of photoexcitation intensity in a range where the red emission associated with the Zn-O complex increases either linearly or superlinearly. The effect is observed in all measured zinc-doped crystals and the behavior is consistent with a model in which the oxygen center successively captures two electrons. In this model the infrared luminescence is associated with the deeply bound electron, while recombination at an oxygen center which has captured both electrons occurs through processes involving these electrons and either a bound or free hole. The experimental data yield recombination rates associated with two-electron processes of the same magnitude as the recombination rate of the deep electron. A value for the second electron energy level ≥ 400 meV is extracted from the measurements. The magnitude of the deep-electron-capture cross section of the oxygen center is evaluated on the basis of the excitation-intensity data and a linear dependence on hole concentration is found from deep-electron-thermalization data. These measurements lead to a value of $\sigma_0 \sim 10^{-17} p / 10^{17}$ cm^2, where p is the hole concentration per cubic centimeter. Similar experiments performed on the Zn-O red band, to attain a more accurate determination of the Zn-O complex electron-capture cross section, yielded a value of $\sigma_{Zn-O} = 2 \times 10^{15}$ cm^2. These two capture cross sections, the maximum values of the impurity-concentration ratio N_{Zn-O}/N_O (obtained from pairing theory), and results of earlier work characterizing Zn-O red luminescence have been combined to obtain an upper limit for the internal quantum efficiency of the Zn-O system. The predicted maximum is $\sim 35\%$ for material annealed at 600 °C. Efficiencies in the 40% range are predicted for equilibrium pairing at 500 °C. Our results are consistent with reported values of maximum-red-luminescence quantum efficiencies and minority-carrier lifetime (τ_L) evaluations. Measurements on a well-characterized sample with a net acceptor concentration of 2.5×10^{17} cm^{-3} yield parameter values of $\tau_L = 13$ nsec and $N_{Zn-O} \simeq 4 \times 10^{15}$ cm^{-3}. On the basis of pairing theory the oxygen-donor concentration is $\sim 7 \times 10^{16}$ cm^{-3}.

I. INTRODUCTION

The efficient radiative center in the red-emitting GaP(Zn,O) system has been identified as a nearest-neighbor zinc and oxygen complex.[1,2] Calculations based on pairing theory[3,4] indicate that only a fraction of the oxygen on phosphorous sites pairs with zinc to form the neutral Zn-O isoelectronic radiative centers. In this paper we consider what effect recombination through the unpaired oxygen sites has on limiting the potential maximum quantum efficiency of the red band. To achieve this aim we evaluate the electron-capture cross sections of both the oxygen and Zn-O centers.

Two basic experimental techniques are used. In the first, the excitation intensity is increased to a level where a substantial fraction of the radiating centers are filled and the corresponding luminescent emission increases sublinearly. These data, along with auxiliary luminescent time decay and minority-carrier lifetime measurements, yield the electron-capture cross section.[5-8] In the sec-

ond technique, the luminescent time decay of the center is monitored as a function of increasing temperature to extract the electron-thermalization time. These data and the principle of detailed balance then enable us to compute the capture cross section. Both the first[6-8] and second[9] methods have been used previously to evaluate the Zn-O complex electron-capture cross section. More reliable parameter values and a better understanding of the system have led us to repeat these measurements with a resultant increased and improved value of 2×10^{-15} cm^2.

The interpretation of the measurements on the oxygen center is less straightforward than with the Zn-O complex. In particular, weak saturation of the infrared luminescence is observed over three decades of excitation intensity before the onset of a sharper sublinear increase. This behavior is consistent with the description of the oxygen center as a two-electron recombination center; an analysis of recombination at such a center is given in a companion paper.[5]

Interpretation of the oxygen-thermalization data requires accounting of retrapping effects and is handicapped by a large uncertainty as to the depth of the oxygen level in the temperature range where thermalization is important (>450 °K). However, from these measurements the oxygen electron-capture cross section is unambiguously demonstrated to increase linearly with hole concentration. The value of the deep-electron-capture cross section obtained by combining this dependence on hole concentration, p, with the magnitude derived from the excitation-intensity data is $\sigma_0 \sim 10^{-17} \times (p/10^{17})$ cm^2. An electron-capture cross section of 10^{-18} cm^2 was derived by earlier workers[10] from saturation measurements in GaP(Zn, O). The initial sublinear behavior at low intensities was not detected in the earlier work and the data were interpreted in terms of a single-electron center.

Oxygen concentrations in the low 10^{17}-cm^{-3} range were deduced in Ref. 10. Values derived from solubility data vary from[11] $\sim 7 \times 10^{16}$ to[12] 2.7×10^{17} cm^{-3}. Chemical measurements are also in this range.[13]

We have not determined the oxygen concentration in this paper, but have evaluated Zn-O complex concentrations of (4 to 8)$\times 10^{15}$ cm^{-3} in samples with net acceptor levels of $\sim 2.5 \times 10^{17}$ cm^{-3}. Using this range and pairing calculations[4] we obtain oxygen-donor concentrations of $\sim 7 \times 10^{16}$ to 1.4×10^{17} cm^{-3} in agreement with the earlier work.

From the values of the two capture cross sections and the previous characterization of the Zn-O center[14] the red quantum efficiency is given in terms of the ratio of Zn-O complex concentration to unpaired-oxygen concentration, N_{Zn-O}/N_O. Since no other competitive centers are considered, these curves define maximum red quantum efficiencies. Experiments are described which are consistent with the predicted results.

We discuss experimental considerations in Sec. II and present the experimental results in Sec. III. The Zn-O complex and oxygen-donor electron-capture cross sections are evaluated in Sec. IV. Curves defining the maximum red quantum efficiency are then calculated and several consistency experiments are described in Sec. V, followed by concluding remarks in Sec. VI.

II. EXPERIMENTAL

A. Apparatus

Data were recorded with both photon-counting and conventional analog techniques. The photon-counting system has been described elsewhere[15]; the central components are a cooled RCA C31000E photomultiplier and a Didac 800 multichannel analyzer. An argon-ion laser pulsed with an acousto-optic modulator gives a modulator-limited system

time of 2.5 nsec. Time decay was measured by the delayed coincidence method.[15,16]

Low-temperature measurements were taken by mounting the samples in a Janis variable-temperature helium-gas-flow Dewar. High-temperature measurements were performed with the sample mounted in the center of a small (about 6-cm long 1.5-cm bore) cylindrical ceramic furnace.

The luminescence-output versus excitation-intensity experiments required steady-state conditions and at the same time avoidance of heating effects at the higher intensities. In this regime long excitation pulses, 500 μsec, were obtained by chopping the laser beam mechanically. Duty cycles of less than 10% were used. Both the Zn-O red band and the oxygen infrared band were monitored. A Corning 7-56 absorption filter was used for the infrared band and these measurements were repeated on a few samples with a silicon-disk filter, 0.15 mm thick. An RCA 7102 S-1 photomultiplier detected emission from both bands and the incident excitation was measured by monitoring a portion of the laser beam with an EG&G SGD-444 photodiode. Pulse heights were read on an oscilloscope. To facilitate measurement of beam diameters and hence excitation intensity, samples were mounted on a micromanipulator, planar with a razor edge on the same mount.

The relative efficiency of the red Zn-O band was obtained by monitoring the peak of the band as the temperature was changed and then measuring the spectra. The spectra were normalized for the system response[15] and the integrated emission was obtained by combining the peak and spectral area measurements. These results were verified for several crystals by directly measuring the integrated signal at a fixed excitation level as a function of temperature. The two measurements agreed closely.

B. Crystal Data

Measurements were performed on a variety of samples. These included solution-grown (Zn, O)-doped p-type GaP crystals with a doping range of 0.007–0.1 mole % zinc and 0–0.1 mole % Ga$_2$O$_3$ (oxygen is inadvertently present in the crystals not purposely doped with Ga$_2$O$_3$). In addition, several (Zn, O)-doped liquid-phase-epitaxial (LPE) layers were measured. A detailed description of the system in which these latter crystals were grown will be given elsewhere.[17] Experiments were also conducted on a (Cd, O) and a carbon-doped solution-grown crystal.

III. EXPERIMENTAL RESULTS

A. Luminescence Emission versus Excitation Intensity

Emission versus excitation-intensity data were taken on several samples. Typical results are
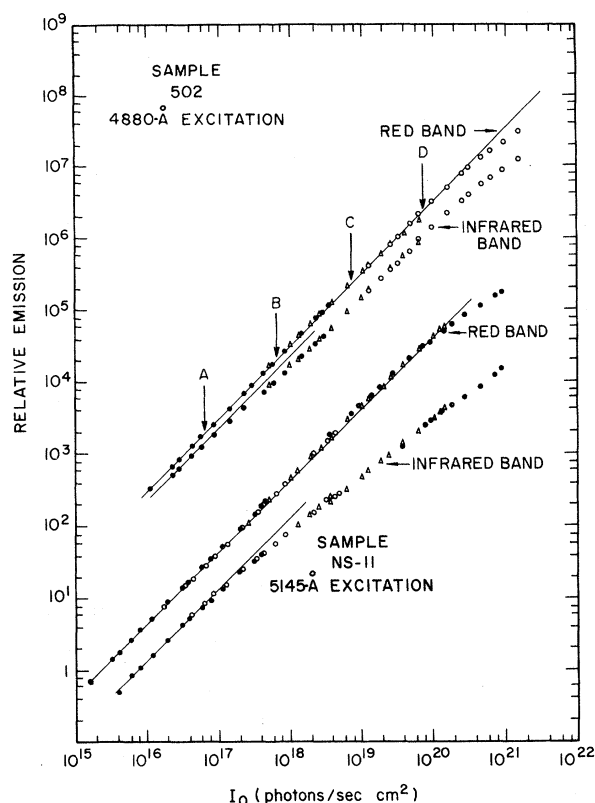
FIG. 1. Luminescent-intensity vs excitation-intensity data for the Zn-O red and oxygen infrared bands on two (Zn,O)-doped GaP samples. The upper sample is a relatively thick solution-grown crystal while the lower sample is a 25-μm LPE layer grown on an n-type substrate. The solid lines denote linear dependence. The arrows on the solution-grown data denote the excitation intensities at which spectra in Fig. 2 were taken.

depicted in Fig. 1 for a (Zn, O)-doped solution-grown crystal and for a similarly doped LPE layer approximately 25 μm thick. Data are given both for spectral bands encompassing the oxygen-associated infrared emission and the efficient Zn-O red luminescence.

Measurements were taken over nearly six decades of excitation intensity. To obtain this range several runs were taken at different beam radii between 25 and 2500 μm. The beam radii at the sample surface were determined from profiles taken with a razor edge. The values were selected to provide large overlap from one run to the next. Reproducibility was good and when necessary beam sizes were adjusted and runs repeated to include critical regions (changes in slope) within a single run.

A few experimental considerations require comment. Deviations from uniform excitation provided by the Gaussian profile of the laser beam and the exponential falloff of intensity within the sample

washout changes in slope of the emission intensity. The data in Fig. 1 were taken using only the central portion of the beam, nominally uniform excitation. The open-circle data for sample 502 in Fig. 1 represent a beam size of 25 μm while the triangular points represent a beam size of 150 μm. The onset of saturation occurred at a much lower intensity for the larger beam. This effect has been explained previously[8] as due to the importance of diffusion in the radial direction for small beam sizes. The diffusion gives the appearance of a larger beam size and results in a nominally higher onset of saturation. In general, saturation of the red band was achieved with beam sizes of 75 μm or larger, in which case the diffusion effect was not consequential.

The measurement on the 25-μm LPE layer helps alleviate the nonuniform behavior in the direction of the beam. The 5145-Å line of the argon-ion laser used for these measurements has a room-temperature absorption length of 30 μm in GaP. The curvature of the infrared data of this sample (Fig. 1) is more pronounced than in the data taken on the relatively thick solution-grown samples.

Spectra on the solution-grown sample at excitation intensities corresponding to the arrows in Fig. 1 are depicted in Fig. 2. The spectra are corrected for the system response and are normalized to the peak of the red band. The relative change in magnitude of the red and infrared bands is in agreement with the data in Fig. 1. The dashed line representing the tail of the red band was obtained by taking the corrected oxygen-associated infrared spectrum from a carbon-doped sample (where there is negligible interference from neighboring bands), normalizing it to the low-energy edge of the infrared band in the zinc-doped sample, and subtracting it from the total spectrum. This process was repeated on several spectra with the same result in all cases. The spectra have been described in some detail to emphasize that the weak saturation of the infrared band is not an artifact due to overlap of the tail of the red band. This latter effect is seen to a certain extent in annealed samples where the infrared luminescence is much lower than the red luminescence and it is manifested during the collection of infrared data by a change in the pulse shape at the highest intensities.

Returning to the excitation-intensity data of Fig. 1, we observe the following:

(i) The infrared emission undergoes a sublinear increase over a substantial range of excitation intensity. The effect is weak compared to the saturation exhibited by both bands at the highest intensities.

(ii) The luminescence of the red band is nearly linear with excitation intensity over most of the
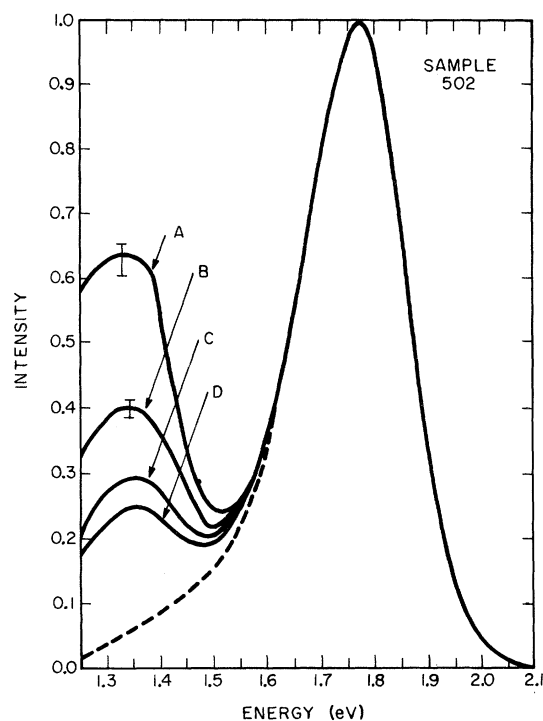
FIG. 2. Spectra on the solution-grown sample corresponding to excitation intensities over three decades in Fig. 1. The spectra were taken with an S-1 response photomultiplier and are corrected.

excitation range where curvature occurs in the infrared band. This result eliminates the possibility of explaining the above observation in terms of instrumental effects. The two curves were obtained sequentially under nearly identical conditions, the only difference being the filter before the photomultiplier. A narrow-band interference filter (100-Å half-power bandwidth) was utilized for

the red-band measurements to ensure that the photomultiplier signal was similar in both cases.

(iii) A slight but definite superlinear variation was observed in the red band.

These effects were, with very little variation, observed in all (Zn, O)-doped samples measured. Table I gives a summary of saturation and other measurements performed on a number of (Zn, O)-doped samples. These results will be discussed in Sec. IV. For the samples of Fig. 1, the superlinear variation in the red band is barely detectable on the scale shown. We find the effect more pronounced for high-efficiency material and plot data from an efficient annealed LPE layer[17] in Fig. 3. Data are also presented for the same sample in the unannealed state. Efficiency is plotted rather than luminescence to allow the use of an expanded ordinate scale. As the infrared band saturates, the red luminescence increases superlinearly in the annealed sample and finally at high excitation levels both bands saturate sharply. In contrast to the annealed state, the red band in the unannealed state does not undergo a superlinear increase. The measurements on the unannealed sample were not carried to a high enough intensity to reach the region of sharp saturation.

Measurements were also performed on a (Cd, O)- and a carbon-doped crystal and these data are given in Fig. 4. The behavior of the infrared band is qualitatively different in both samples than that observed in the zinc-doped crystals. In particular, the cadmium-doped sample displays only a small sublinear effect while the infrared band of the carbon-doped sample increases superlinearly before saturating.

The room-temperature spectrum (un-normalized) of the carbon-doped sample is given in Fig. 5. This sample has a very weak red band which lies

TABLE I. Summary of experimentally derived parameters.

Sample	p (cm^{-3})	τ_L (nsec)	τ_0 (μsec)	τ_t' [a] (nsec)	Excitation α (cm^{-1})	I_0^* (red)[b] photon/sec cm^2	I_0^* (ir)[b] photon/sec cm^2	σ_{Zn-O} [c] (cm^2)	σ_0 [c] (cm^2)
502	1.8×10^{17}	5	72	160	1000	4×10^{19}	10^{17}	2.5×10^{-15}	1×10^{-17}
NES-17P A2	2.5×10^{17} $(N_A - N_D)$	7	60	160	300	7×10^{19}	10^{17}	3×10^{-15}	3×10^{-17}
NES-17P C3 Unannealed	2.5×10^{17} $(N_A - N_D)$	4.5	50	160	300		1.5×10^{17}		4×10^{-17}
NES-17P C3 Annealed	2.5×10^{17} $(N_A - N_D)$	13	50	160	300	1.5×10^{19}	2×10^{16}	3×10^{-15} [d]	10×10^{-17}
7161	6.2×10^{17}	5	20	120	300	10^{20}	5×10^{17}	4×10^{-15}	2.5×10^{-17}
NES-11	6.8×10^{17}	7	30	115	300	1.5×10^{20}	10^{17}	2×10^{-15}	5×10^{-17}
5132	9.3×10^{17}	6	8	90	1000	10^{20}	10^{17}	1.3×10^{-15}	8×10^{-17}

[a] τ_t' is defined by Eq. (3).

[b] For definition of I_0^* (red) and I_0^* (ir) see Eqs. (5) and (10) and adjacent text.

[c] The cross-section values σ_{Zn-O} and σ_0 were derived

from the saturation data.

[d] Based on calculated curves from sample parameters rather than approximate solution of Eq. (5).
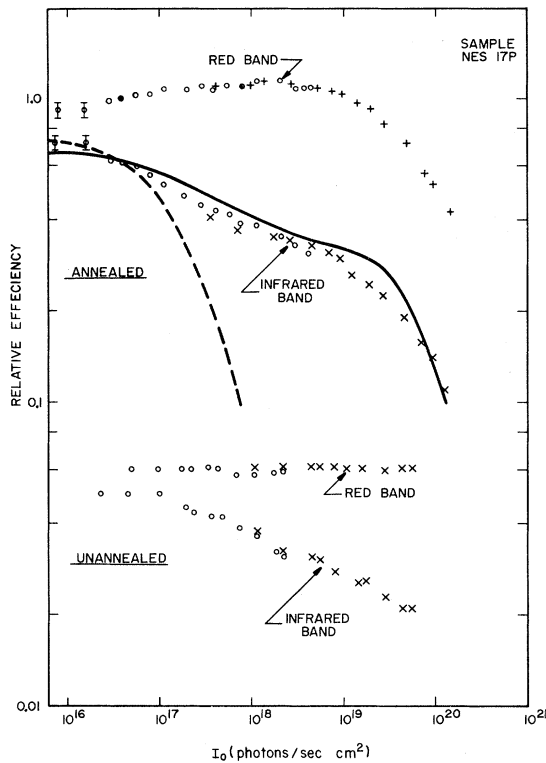
FIG. 3. Red and infrared efficiencies versus excita-
tion intensity for a LPE (Zn,O)-doped p layer. The the-
oretical curves are discussed in Sec. IV. All experi-
mental data are arbitrarily placed on the ordinate scale
and the computed curves are normalized to the data.
The two-electron model of Ref. 5 was used to compute
the solid curve with $n_t/n_0 = 3$, $\tau_{2n}/\tau_0 = 0.5$, and (σ_0/σ_k)
$\times (1 + \tau_{2n}/\tau_{kn} + \tau_{2n}/\tau_{20}) = 0.025$. The dashed line indicates
the infrared response using a single-electron model.
For this curve $n_t/n_0 = 300$.

close to the energy of the Zn-O and Cd-O lumines-
cence. Its characteristics are similar to an un-
identified band previously reported by other
workers.[18,19] The association of the infrared band
in this sample with the oxygen center is unequivo-
cably demonstrated by time-decay measurements
(Sec. III B). Corning 4-77 and 2-73 absorption
filters were used to observe the red luminescence
in the carbon sample; this broad-band combination
was necessitated by the low signal level available.

B. Thermalization Data: Oxygen Center

Time-decay data are plotted in Fig. 6 for the
infrared band of the (Zn, O)-doped solution-grown
sample, for which intensity data were given in
Fig. 1. These data are taken through a narrow-
band interference filter (100-Å half-power band-
width) centered at 9000 Å. The initial fast compo-
nent at low temperatures (300–400 °K) represents
the decay of the tail of the red band. The red band

is enhanced relative to the infrared band since only
relatively short, ~3 μsec, excitation pulses are
generated by the acousto-optic modulator and the
slow-decaying infrared band does not achieve its
steady-state intensity. As the temperature in-
creases the red band rapidly attenuates because
of thermalization of electrons from its relatively
shallow electron level, and the initially fast-decay
component disappears. With further increase in
temperature the thermalization of electrons on
the deep oxygen site becomes relevant and the slow
exponential component becomes faster. Note the
initial fast decay that now occurs in the high-tem-
perature range. A possible interpretation of this
effect is given in terms of the recombination model
of two electrons on an oxygen site as discussed in
Sec. IV.

In Fig. 7 the $1/e$ decay time of the slow infrared
component is plotted versus reciprocal tempera-
ture for three samples including the carbon-doped
crystal. Measurements were taken on three addi-
tional (Zn, O)-doped samples and similar results
were obtained. The shift in absolute value of time
decay between the samples correlates inversely
with the free hole or net acceptor concentration.

C. Thermalization Data: Zn-O Complex

Figure 8 depicts $1/e$ time decay data in the Zn-
O red band for two samples with room-tempera-
ture hole concentrations of 4×10^{17} and 1.5×10^{18}
cm^{-3}. The motivation of these measurements was
to obtain thermalization data for the red band and
eliminate discrepancies that have arisen in earlier
work (discussed in Sec. IV). Samples were select-
ed which were not purposely doped with oxygen.
Hence, the concentration of Zn-O complexes is
low and the fraction of thermalized electrons that
is recaptured by the complexes is negligible. Such
samples enable an accurate determination of the
electron-thermalization time.[14]

D. Efficiency versus Temperature Data

To obtain information as to the nature of the
nonradiative center or centers competing with the
Zn-O complex the relative radiative efficiency of
the red band was monitored on a number of sam-
ples as a function of temperature. The results
are shown in Fig. 9. Two types of behavior are
observed. In the low-doped samples the efficiency
goes through or approaches a minimum at about
150 °K before the steep falloff above 250 °K due to
thermalization of electrons from the Zn-O com-
plex. The minimum is most pronounced in the
sample not doped with oxygen. In the higher-
doped samples the efficiency decreases monotoni-
cally above ~70 °K with increasing temperature.
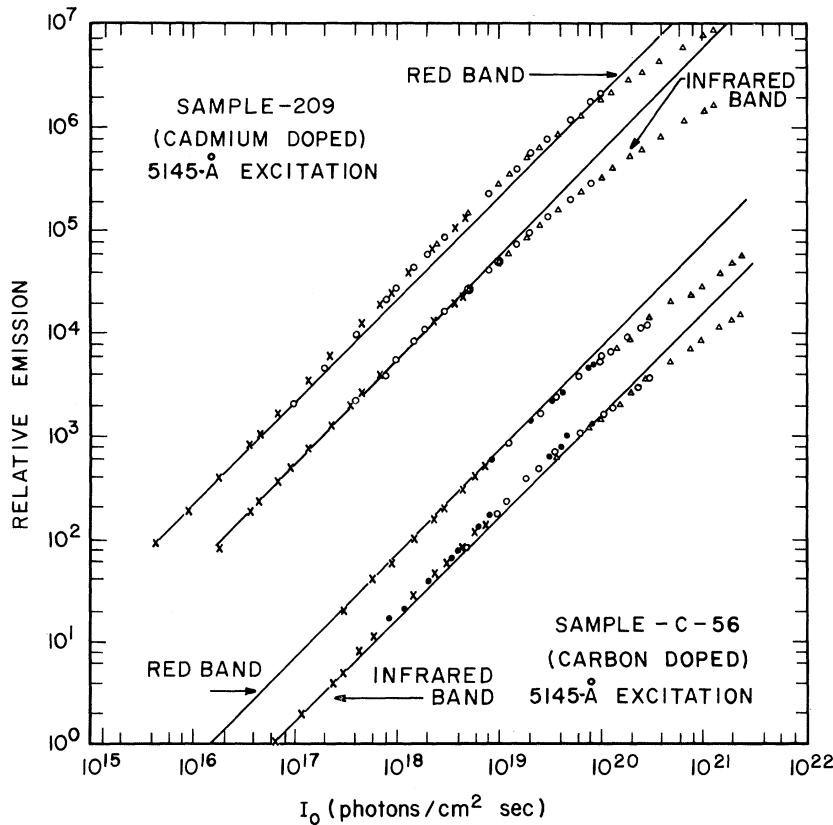This latter variation has been described by pre-

FIG. 4. Luminescent-intensity vs excitation-intensity data on (Cd, O)-doped sample (upper) and a carbon-doped sample (lower). The red band of the (Cd, O)-doped sample is the Cd-O excitonic band while the red band of the carbon-doped sample is unidentified.

vious workers.[20,21] The increase in efficiency with temperature at the lowest temperatures results because of thermalization of electrons from shallow donors and the quenching of the associated green pair band.[20,22]

A functional variation similar to that observed in the low-doped samples has been derived[5] on the basis of a model in which the radiative center competes with a deep neutral acceptor, which binds an exciton. Rapid recombination occurs at the nonradiative center through an Auger process.

The data in Fig. 9 lend credence to the relevance of this model, but further evidence is required. Many more samples must be measured before the
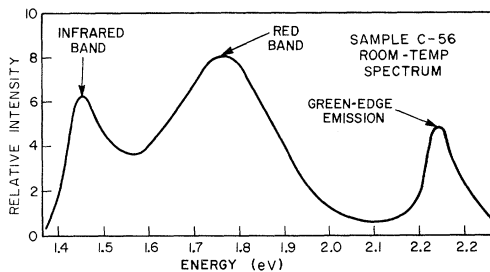

FIG. 5. Spectrum of the carbon-doped sample depicting the oxygen infrared band, the unidentified red band, and the green edge emission. The spectrum was taken with an RCA 31000E photomultiplier and is uncorrected. The apparent shift of the infrared band to higher energies relative to the spectra of Fig. 2 is not real.
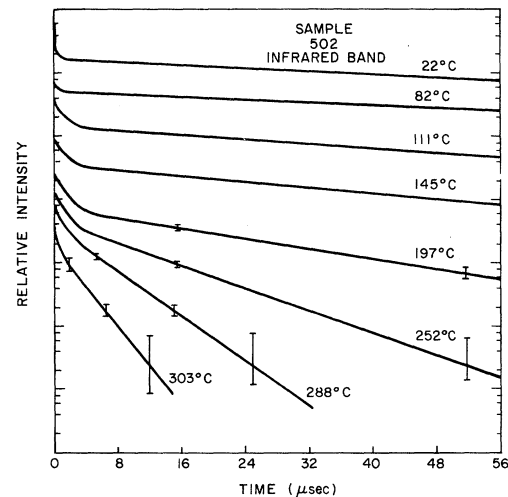

FIG. 6. Luminescent time-decay data with temperature as a parameter. The initial fast component in the temperature range 22–111 °C is due to the tail of the red band. The fast component at higher temperature may be due to a two-electron process at the oxygen center as is discussed in Section IV B 2.
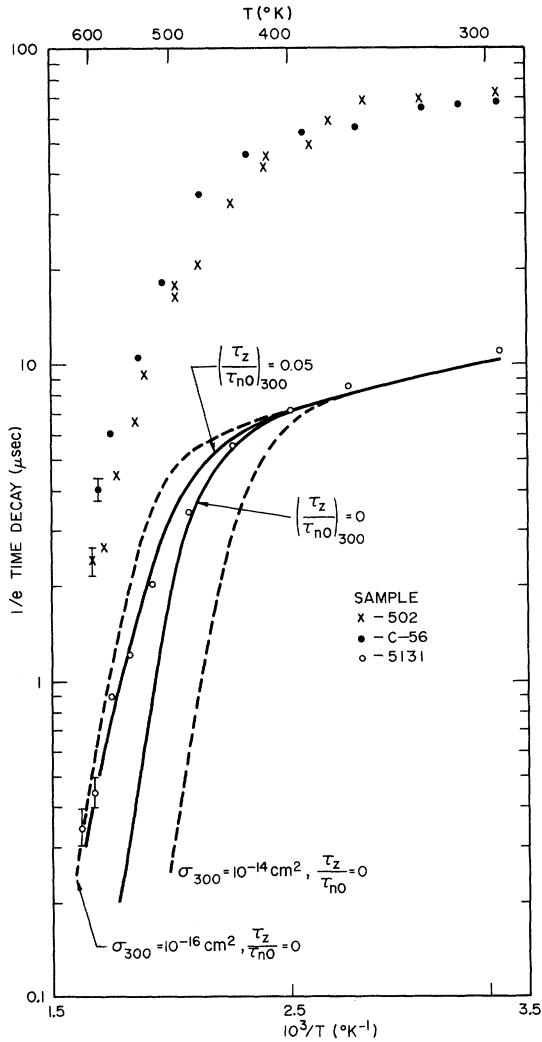
FIG. 7. $1/e$ decay time of infrared luminescence vs reciprocal temperature. Only the slow component is taken into account in cases with an initially fast decay. Data are given for three samples, the upper pair have free-hole carrier concentrations of $\sim 1.5 \times 10^{17}$ cm^{-3} while the lower sample has a carrier concentration of 1.1×10^{18} cm^{-3}. The theoretical curves are discussed in Sec. IV. A value of $\sigma_0 = 10^{-16}$ ($p/10^{17}$) was used in the calculations of the solid curves. The decay component τ_0 correlates with hole concentration (Ref. 33) and a variation $\tau_0(300/T)^{1.2}$ was introduced on the basis of curves found in H. C. Casey, Jr., F. Ermanis, and K. B. Wolfstirn [J. Appl. Phys. **40**, 2945 (1969)].

qualitative difference between the behavior of low- and high-doped samples can be generalized.

E. Minority-Carrier Lifetime Measurements

The minority-carrier lifetime is required for quantitative interpretation of the luminescent

saturation data. Three techniques were used—measurement of the green-luminescence time decay,[23] impulse excitation,[24] and measurement of the diffusion length through electron-beam scanning of a p-n junction.[25] This latter technique is suitable for measurements on the LPE layers which are grown on n-type substrates.

The green-luminescent time decay gives a direct measure of the minority-carrier lifetime because the electrons involved in the near-band-edge emission are in equilibrium with the conduction-band electrons during the time span of interest.[23]

Impulse excitation consists of exciting the sample with an extremely short pulse and monitoring the rise time of the red luminescence. This rise time is a direct measure of the minority-carrier lifetime if the lifetime is much shorter than the red-luminescence decay time.

Several samples were measured via two techniques and the agreement was good. The values are given in Table I.
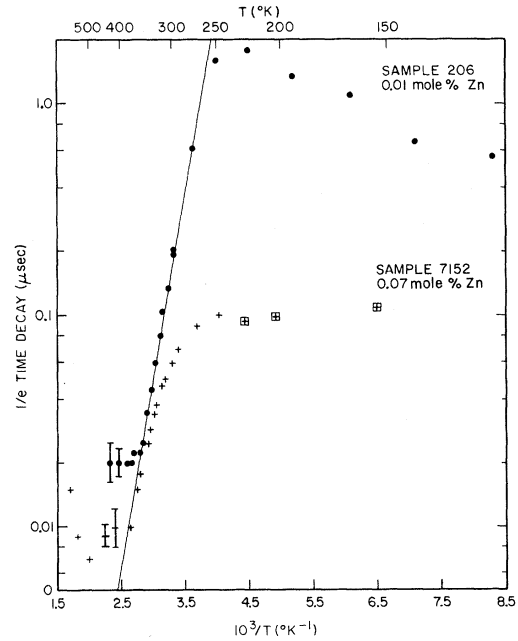

FIG. 8. $1/e$ time of Zn-O red luminescence vs reciprocal temperature plotted for data from two zinc-only-doped solution-grown crystals. The boxed-in data points at low temperatures on the higher doped sample indicate nonexponential data which may be due to another underlying red band. The error bars at higher temperatures also indicate nonexponential data which are due to a transition in the time–decay data from a measure of rates out of the Zn-O center to a measure of the minority-carrier lifetime. The transition occurs when the electron-thermalization time from the complex becomes faster than the minority-carrier lifetime.
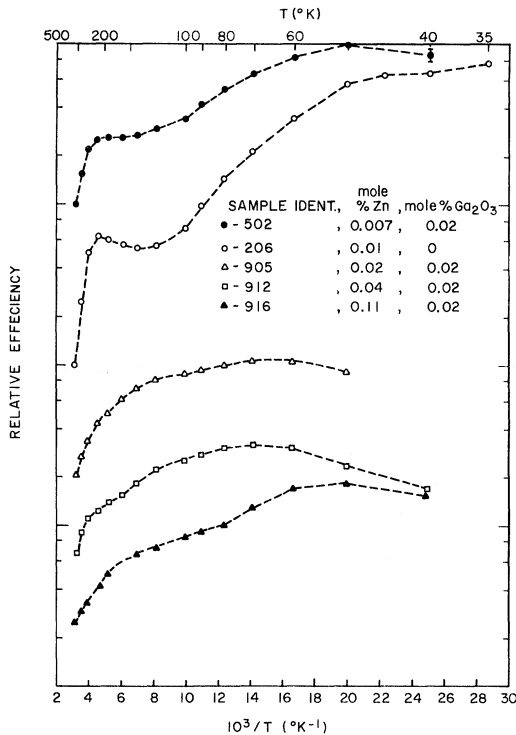
FIG. 9. Relative efficiency of the Zn-O red lumines-
cence vs reciprocal temperature for several solution-
grown crystals of various doping levels. The data are
shifted for convenience of viewing, the lowest zinc level
at the top and the highest at the bottom. This order is
arbitrary and does not reflect the relative efficiency of
one sample with respect to another.

IV. EVALUATION OF Zn-O COMPLEX AND OXYGEN-DONOR ELECTRON-CAPTURE CROSS SECTION

This section is divided into two subsections.
In Sec. IV A the Zn-O-complex electron-capture
cross section is evaluated. Section IV B continues
with the evaluation of the oxygen electron-capture
cross section. In Sec. V, the consequence of these
two values is discussed with regard to the effect
of oxygen as a limiting factor on the quantum effi-
ciency of the red-emitting Zn-O system.

A. Evaluation of the Zn-O Complex Electron-Capture Cross Section

1. Thermalization Data

The Zn-O complex electron-capture cross sec-
tion is first calculated utilizing the data in Fig. 8.
The sharp drop in red-luminescence time decay at
250 °K results from thermalization of electrons
out of the complex into the conduction band. Inef-
ficient samples which were not purposely doped
with oxygen were selected to minimize the Zn-O-
complex concentration and minimize retrapping of

thermalized electrons. The room-temperature
free hole concentrations of the upper and lower
samples in Fig. 8 are, respectively, 4×10^{17} and
1.5×10^{18} cm^{-3}; the time-decay difference at low
temperatures results from larger Auger and radi-
ative rates in the higher-doped sample. At higher
temperatures where the thermalization process
dominates, the decay times of the two samples
approach the same value. The break at elevated
temperatures from an exponentially decreasing
variation with reciprocal temperature represents
the point at which the thermalization time is
comparable to the minority-carrier lifetime. The
luminescent decay is nonexponential with time in
this transition region. Above this temperature the
red center is in rapid communication with the con-
duction band and the red-luminescent decay time
measures the minority-carrier lifetimes. Other
workers[26] have also reported the utilization of this
high-temperature plateau for evaluating the minor-
ity-carrier lifetime in GaP(Zn, O). The room-
temperature minority-carrier lifetime on the
lower-doped sample measured by means of the im-
pulse-excitation technique[24] is ~ 20 nsec, in good
agreement with the high-temperature value in Fig.
8. The increase of minority-carrier lifetime in
the temperature region 500–600 °K correlates
with the thermalization of electrons from the oxy-
gen center (see Fig. 7).

From the principle of detailed balance the elec-
tron-capture cross section σ_t is related to the
thermalization time τ_{tn} through the expression

$$\tau_{tn} = g\, e^{E_t / kt} / \sigma_t\, N_c v_{\text{th}} \ , \qquad (1)$$

where g is the degeneracy factor of the center,
E_t the energy level with respect to the conduction
band, and N_c the conduction-band density of states
equal to $1.6 \times 10^{19} (T/300)^{3/2}$ cm^{-3}. We place $g = 2$;
the degeneracy due to the multiplicity of conduc-
tion-band minima is split by the Zn-O complex
local field.[27] The thermal velocity $v_{\text{th}} = 2 \times 10^7$ cm/
sec and the conduction-band density of states are
computed using an effective electron mass of
$0.37 m_0$.[28]

The slope of the line through the data points in
Fig. 8 represents an activation energy of 340 meV.
Using Eq. (1) and assuming the complex capture
cross section $\sigma_t \rightarrow \sigma_{\text{Zn-O}}$ to be temperature indepen-
dent (a reasonable assumption for a neutral center),
we obtain a value of 285 meV for the Zn-O electron
energy level E_t at room temperature. This value
is slightly higher below room temperature and
lower above room temperature. The difference
between the activation energy and the value for E_t
arises from the T^2 dependence of the product
$N_c v_{\text{th}}$. The value for E_t is in good agreement with
the low-temperature value of 300 meV deduced
from optical measurements,[27] and values deduced

from photocurrent measurements.[9] The complex energy level was also previously deduced from the thermalization time, the previous values of the capture cross section,[7-9] and Eq. (1) to be 0.24 ± 0.02 eV at room temperature.[10,14] The higher capture cross section determined here by two techniques eliminates the previous inconsistency between the low-temperature optical result and the deduced room-temperature energy depth.

The capture cross section σ_{Zn-O} as calculated from Eq. (1) equals 2×10^{-15} cm^2. In previous work capture cross sections in the range (1.5 to $6.7) \times 10^{-16}$ cm^2 had been derived from saturation measurements[7,8] and in Ref. 9 a capture cross section of 6×10^{-16} cm^2 was derived from photocurrent measurements. The discrepancy in the latter case stems from the assumption of six conduction-band minima rather than three, and the deduction of a longer thermalization time, apparently because of the neglect of retrapping effects. The difference in the former case is a result of several factors which we discuss in more detail as a means of introducing the concepts necessary to interpret both the red and infrared excitation-intensity data.

2. Excitation-Intensity Data

The equation describing the steady-state filling of a single-electron center in terms of the minority-carrier concentration n is

$$n\sigma_t v_{th} N_t (1 - N_t^e/N_t) = N_t^e/\tau_t + N_t^e/\tau_{tn} , \qquad (2)$$

where N_t is the concentration of the centers, N_t^e is the concentration of centers with captured electrons, and τ_t is the parallel combination of radiative and nonradiative recombination times. The thermalization time τ_{tn} into the conduction band was defined earlier. Thus the left-hand side of the equation is the rate of capture into the center and the right-hand side is the rate of loss from the center. The equation can be rearranged to give the expression

$$\frac{N_t^e}{N_t} = \frac{n/n_t}{1 + n/n_t} , \qquad (3)$$

where

$$n_t = 1/\sigma_t \tau_t' v_{th} , \quad 1/\tau_t' = 1/\tau_t + 1/\tau_{tn} .$$

When the minority-carrier concentration equals n_t, the centers are half filled and the luminescence output increases sublinearly with increasing excitation. Specification of the competitive centers and solution of a set of simultaneous equations leads to the description of the minority-carrier concentration as a function of generation rate. This problem was solved in Refs. 7 and 8 under the assumption that the competing centers did not saturate before the red-luminescent center. There

is, however, experimental evidence[8,29] that most of the competitive centers do saturate before or simultaneous with the Zn-O complex. Further evidence is provided by the superlinear behavior of the red band observed in Figs. 1 and 3. Under these conditions the appropriate solution for the onset of saturation is similar to a solution assuming no competitive centers[8]:

$$G^*\tau_L \approx n_t , \quad G^* = \alpha I_0^*(1 - R) \qquad (4)$$

where τ_L is the low-level minority-carrier lifetime. The minority-carrier generation rate G in this instance is specified by the product of the absorption coefficient α and the incident intensity at the onset of saturation I_0^* of the excitation beam. The factor $1 - R$ represents a reduction of intensity because of reflection $R \approx 0.3$. From the definition of n_t and Eq. (4) we have

$$\sigma_t \simeq \frac{1}{\alpha I_0^* \tau_t' \tau_L v_{th}(1 - R)} . \qquad (5)$$

The value of I_0^* is determined from the intersection of the slopes of the linear and sublinear portions of the experimental data. The value of τ_t' is computed from known parameter values[14] and is given in Table I. The computed value of the Zn-O complex electron-capture cross section is also tabulated and falls in the range (1 to $4) \times 10^{-15}$ cm^2, in agreement with the value deduced from the thermalization data.

The discrepancy between the present results and earlier saturation measurements[7,8] arises from three problem areas: (i) The importance of thermalization was not appreciated in the previous work and, particularly for the high-doped material utilized in that work ($p \approx 8 \times 10^{17}$ cm^{-3}), the value of τ_t' was approximately 50% too high. (ii) The value of the minority-carrier lifetime τ_L is determined more accurately in the present work. In Ref. 7 a range of values was assumed while in Ref. 8 the values were determined through an indirect excitation spectral technique.[8,20] (iii) In Ref. 8, a range of capture cross sections was given which depended upon the nature of the competitive centers. From the above discussion the upper end of the range is the appropriate choice. In addition to these considerations, the aperturing of the excitation beam, the measurement in some cases of thin layers, and the use of larger excitation-beam diameters leads to a sharper definition of the saturation region and reduces the experimental scatter.

B. Evaluation of the Oxygen-Center Electron-Capture Cross Section

1. Thermalization Data

The electron-capture cross section of the substitutional oxygen donor has been evaluated as with

the Zn-O complex, through both thermalization and excitation-intensity measurements.

Referring to Fig. 7 where the thermalization data of the oxygen center are presented for three samples, and comparing these data with that of Fig. 8, we observe that the oxygen decay times do not approach the same value at high temperature as is the case with the Zn-O complex. One finds from the six samples measured that the thermalization time is faster for the higher-doped sample and is inversely proportional to the hole or acceptor concentration. Equation (1) then implies a capture cross section $\sigma_t - \sigma_0$ proportional to the hole or acceptor concentration. This observation is in agreement with an Auger capture mechanism suggested by Dean and Henry.[30] These authors established that the first excited state of the oxygen donor is ~ 50 meV below the conduction band compared to the ground-state value of 895 meV at low temperatures.[31] The large energy loss of a captured electron is assumed to be imparted to a hole which is ejected deep into the valence band, and thus the dependence of capture cross section on free hole or acceptor concentration.

A quantitative dependence of the capture cross section on temperature is obtained by considering the expression which describes the measured infrared time decay,[5,14]

$$\frac{1}{\tau_{\text{meas}}} = \frac{1}{\tau_0} + \frac{1}{\tau_{0n}(1 + \tau_z/\tau_{n0})} \quad ,$$

$$\tau_z = \tau_{nt}(1 + \tau_t/\tau_{tn}) \quad . \tag{6}$$

In the above, τ_0 and τ_t are the decay times from the oxygen and competitive centers, respectively, to the valence band. The corresponding thermalization times into the conduction band are τ_{0n} and τ_{tn} while the capture times are given as τ_{n0} and τ_{nt}. If samples can be selected such that $\tau_z/\tau_{n0} \rightarrow 0$, then thermalized electrons are not recaptured and the observed time decay approaches the thermalization time τ_{0n} at elevated temperatures. This was the situation attained for the red-band measurements given in Fig. 8. However, in the case of the infrared data, the competitive centers are shallow compared to the oxygen center and become less effective with increasing temperature. Under these circumstances retrapping onto the oxygen center is important and the observed activation energy is effectively the difference between the energy of the oxygen center and the competitive center. The activation energy in Fig. 7 is of the order of 400 meV and this is close to the difference in energies of the oxygen center and Zn-O complex at these temperatures (450–600 °K). The carbon-doped sample behaves in a similar manner and the competitive centers in this case may be

related to the unidentified red band (Fig. 5).

As a result of the retrapping problem the energy of the oxygen center cannot be determined from the thermalization data and must be obtained from other sources.

The band-gap variation in GaP is given by the relationship[32]

$$E_g = 2.338 - \frac{6.2 \times 10^{-4} T^2}{T + 460} \text{ eV}. \tag{7}$$

Spectral measurements by Bhargava[33] up to 440 °K indicate that the oxygen-donor level varies little with respect to the valence band and thus its absolute variation with respect to the conduction band is close to the change in the band gap. In this situation the value of E_0 is 822 meV at 300 °K and 685 meV at 600 °K. These energies represent an electron on an isolated oxygen site. In fact, Coulomb repulsion from neighboring ionized Zn acceptors results in a considerable shift of E_0 to lower values.[31] If we perform our calculations with a value of E_0 that is 100 meV lower than the above values the resulting capture cross section represents a lower bound *if* the oxygen level is pinned to the valence band. The degeneracy of the center g lies between 2 and 6, depending upon the degree it has been split by local fields of neighboring impurities. We arbitrarily assume $g = 2$ in line with obtaining a lower bound to the capture cross section. The curves in Fig. 7 were computed using these values and Eqs. (1) and (6). A competitive center energy level of 300 meV was utilized. The resulting capture cross section is $\sigma_0 \sim 10^{-16}(p/10^{17})$ cm^2. Despite the choice of parameter values aimed at obtaining a lower bound for the capture cross section, the excitation-intensity data discussed in Sec. IV B 2 yield a value an order of magnitude lower than that deduced here and we conclude that in the temperature range 450–600 °K the oxygen level is ~ 100 meV closer to the conduction band than was assumed above.

2. Excitation-Intensity Data

The luminescence emission data of the infrared band in zinc-doped samples, as given in Figs. 1 and 3, show a characteristic weak saturation over approximately three decades before the onset of a sharper sublinear decrease. Observation of the behavior of the red band over the same interval rules out the possibility that the minority-carrier concentration is increasing in an anomalous fashion with increasing excitation over this range. The oxygen saturation data therefore cannot be explained in terms of the filling of a single-electron center as expressed by Eq. (3).

Plausibility arguments have been put forth[34] concerning the stability of excitons bound to neu-

tral donors and acceptors and a number of shallow donor sites in GaP have been experimentally found[35,36] to satisfy this prediction. Dean and Henry[30] observed saturation behavior of the oxygen internal luminescent band which was consistent with a model allowing a bound exciton on the neutral oxygen site. An analysis of the recombination kinetics at a center which captures two electrons is given in an accompanying paper.[5]

We briefly review the features of this model relevant to the present discussion. The second electron retards saturation of the center by decreasing the effective recombination time with increasing intensity. At low intensities all recombination takes place through the deep electron. As the excitation increases the population of the second electron increases quadratically and an increasing fraction of the recombination current is shunted through the two-electron processes. The

superlinear increase of this recombination manifests itself as a sublinear increase in the luminescence associated with recombination of the deep electron. It is to this mechanism we attribute the excitation-intensity behavior of the infrared band. Two parameters describe the functional variation of the luminescence with increased generation. The first is the ratio of the deep-electron decay time τ_0 to a time τ_{2n} which describes processes in which the initial state consists of two electrons and the final state consists of one electron in the conduction band. The second parameter involves the ratio of the shallow-electron-capture cross section to the deep-electron-capture cross section σ_k/σ_0.

From Ref. 5 we write an expression, analogous to Eq. (3), which describes the deep-electron concentration in terms of the minority-carrier concentration,

$$\frac{N_0^e}{N_0} = \frac{n/n_0}{1+n/n_o\{1+(\tau_0/\tau_{2n}-1)\left[n/n_0+(\tau_o/\tau_{2n})(\sigma_o/\sigma_k)(1+\tau_{2n}/\tau_{kn}+\tau_{2n}/\tau_{2o})\right]^{-1}\}} \quad , \qquad n_0=1/v_{\text{th}}\sigma_0\tau_0 \ . \qquad (8)$$

The capture cross-section parameter is modified by a factor which includes a thermalization time τ_{kn} of the shallow electron and a time τ_{20} which describes processes with two initial electrons and a final state in which the deep-electron level is occupied. In Ref. 5 families of curves are given in which the two parameters are varied. The parameters affect the functional variation in a near independent manner and values of $\tau_{2n}/\tau_0 \simeq 0.5$ and

$$\sigma_0/\sigma_k(1+\tau_{2n}/\tau_{kn}+\tau_{2n}/\tau_{2D}) \simeq 0.025$$

are obtained which are accurate to within a factor of 2. Using these parameter values we calculate the onset of sublinear behavior to occur when

$$G^*\tau_L \approx 0.005n_0 \ . \qquad (9)$$

A comparison with Eq. (4) indicates the extent to which the saturation characteristic is perturbed by recombination involving the second electron. The expression for the deep-electron-capture cross section is

$$\sigma_0 \simeq \frac{0.005}{\alpha I_0^* \tau_0 \tau_L v_{\text{th}}(1-R)} \ . \qquad (10)$$

Values of σ_0 are given in Table I for several zinc-doped samples. There is much scatter in the results, but not an unreasonable amount considering the nebulous nature of the onset of saturation. A value of $\sigma_0 \sim 10^{-17}(p/10^{17})$ cm^2 is extracted from a combination of these results and the linear dependence of capture cross section upon hole concentration, deduced from the thermalization data.

The thermalization measurements yielded an apparent lower bound for the deep-electron-capture cross section of $\sigma_0 \sim 10^{-16}(p/10^{17})$ cm^2 when the oxygen level was assumed pinned to the valence band. The discrepancy between this value and the value given above possibly originates with the deep-electron oxygen level being shallower than was assumed.

The excitation-intensity data also yield information on the energy level of the second electron. If we assume $\tau_{2n}/\tau_{kn} \gg 1$, the product of the two parameters in Eq. (8) is

$$\sigma_0\tau_0/\sigma_k\tau_{kn} \approx 0.05 \ .$$

The values of σ_0 and τ_0 are known and using the principle of detailed balance [Eq. (1)], the value of the product $\sigma_k\tau_{kn}$, and accounting for the possible failure of the above inequality, the second-electron energy level is computed to be $\geqslant 400$ meV. Although the system is dissimilar from the two other identified neutral oxygen centers in GaP, the Zn-O and Cd-O complexes, we note that the binding energy of an electron in these systems is, respectively, ~ 300 and 400 meV.

The initial fast infrared component observed at high temperatures (Fig. 6) is also consistent with the two-electron model. Under moderate or high excitation conditions where a substantial concentration of deep electrons is found, thermalized electrons can be captured by the shallow second-electron state. This electron pair in combination with a hole recombines through the two-electron

processes accounting for an initial rapid depletion of deep electrons which is monitored through observation of the infrared radiation. As the deep electrons decay, the capture of shallow electrons becomes less probable and the time decay reverts to the slow mode.

The carbon- and cadmium-doped crystal data in Fig. 4 remain to be explained. The infrared band in these crystals does not exhibit the characteristic behavior observed in the zinc-doped crystals. Two possible explanations are a perturbation in the minority-carrier concentration due to the filling of another major center, or a perturbation of the system parameter values, in particular the ratio τ_0/τ_{2n}, due to a dependence upon the specific acceptor. The first explanation suffices to explain the cadmium data in view of the large superlinear effect in the red band which extends over three orders of magnitude of excitation intensity. The same reasoning is apparently not applicable to the carbon-doped sample. An increase of a factor of 2 or 3 in the time τ_{2n} relative to the infrared decay time would explain these data, but a definitive answer awaits measurements on a series of carbon-doped samples. The red band on the carbon-doped sample was monitored for an additional two orders of magnitude lower in intensity than indicated in Fig. 4. A quadratic dependence would indicate a possible tie-in with two-electron recombination at the oxygen site, but a linear dependence was observed at these lower levels.

V. OXYGEN CENTER AS LIMITING FACTOR ON RED-LUMINESCENT QUANTUM EFFICIENCY IN GaP(Zn,O)

The consequences of the measured capture cross sections on the ultimate red quantum efficiency in the GaP(Zn, O) system are presented in Sec. V A. Several experimental consistency arguments are examined in Sec. V B, while in Sec. V C several problems and inconsistencies are discussed which must be resolved before the role of the oxygen donor in GaP is completely understood.

A. Thermodynamic Limit on Internal Red-Luminescent Quantum Efficiency

The measurement of the minority-carrier electron-capture cross sections for the O and Zn-O centers allows some definitive statements to be made about the maximum attainable efficiency in GaP(Zn, O). These results follow from thermodynamic limitations on the maximum concentration ratio of Zn-O to O centers at a given Zn level and a given annealing temperature.

In the considerations below, we assume an impurity system in the GaP matrix containing only Zn and O with the oxygen donor providing the only competitive center to the Zn-O complex. We are

not suggesting that these conditions are realized in most present crystals, but rather emphasizing that this is an ideal that has in fact been approached in the best available material.

The kinetic model of the Zn-O red-luminescent quantum efficiency was parametrized in Ref. 14 in terms of the capture time of the nonradiative centers to the capture time of the Zn-O complex. On the basis of this model, Fig. 10 similarly depicts the conduction-band internal quantum efficiency versus free-hole concentration for various ratios of N_{Zn-O}/N_O (solid curves). A Zn-O complex electron-capture cross section of 2×10^{-15} cm^2 and an oxygen deep-electron-capture cross section of $10^{-17}(p/10^{17})$ cm^2 were used in these computations. Some error is expected because of the uncertainty of the latter value, but the value is considered to be a lower bound, which in turn leads to an upper bound on the efficiency. The dashed curves represent limits on the N_{Zn-O}/N_O ratio at different annealing temperatures based on the pairing calculations of Wiley.[4] These latter calculations were performed in terms of total zinc concentration. To translate the results into the Hall-determined hole concentration p requires consideration of
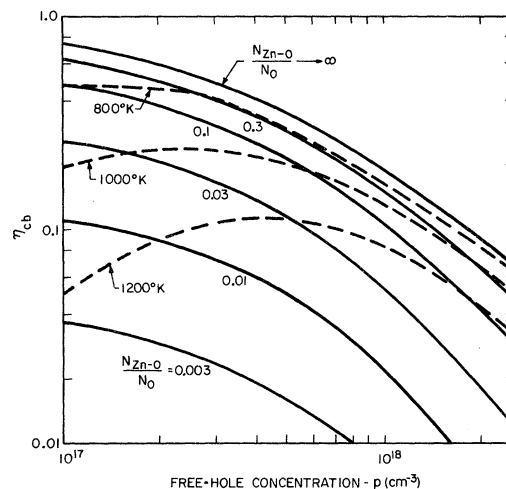

FIG. 10. Red-luminescence quantum efficiency of conduction-band electrons η_{cb} as a function of free hole concentration. The solid contours represent constant values of the ratio of the Zn-O complex concentration N_{Zn-O} to the oxygen-donor concentration N_O. These curves were plotted using Zn-O complex and oxygen-donor electron-capture cross sections of 2×10^{-15} cm^2 and $10^{-17}(p/10^{17})$ cm^2, respectively, and the relationship between η_{cb}, p, and the ratio of a competitive center capture time to the Zn-O capture time given in Ref. 14. The dashed lines represent the maximum attainable red-luminescence efficiencies assuming equilibrium pairing conditions. They are obtained from pairing calculations (Ref. 4) of the maximum values of N_{Zn-O}/N_O as a function of zinc concentration.

compensation as well as the fraction of ionized acceptors. For the purposes of this calculation p was set equal to $0.7N_{Zn}$.

A maximum internal quantum efficiency of 35% is calculated for samples annealed at 600 °C. A value in the 40% range is predicted if equilibrium pairing is achieved at 500 °C. Deliberate compensation of the material could lead to higher Zn-O complex concentration for given hole and oxygen concentrations; this approach has been attempted with some measure of success[37] and would potentially increase the maximum achievable quantum efficiency.

B. Consistency Experiments

A number of measurements have been performed on the annealed sample in Fig. 3 to test the consistency of our results. This sample has an external photoluminescent quantum efficiency close to the reported maximum.[38] In the following paragraphs we review: (i) the predicted and measured photoluminescent quantum efficiencies; (ii) the measured Zn-O complex concentration, the oxygen concentration deduced from pairing theory, and earlier determinations of both values; and (iii) the red and infrared saturation results.

The internal quantum efficiency of red-emitting GaP(Zn, O) material can be computed from a measurement of the hole concentration and the Zn-O-complex luminescent time decay.[14] This calculation is possible because of the functional dependency of the red-luminescence decay time at a given hole concentration on the retrapping of thermalized electrons. The sample in Fig. 3 has a red decay time of 440 nsec and a hole concentration of 2×10^{17} cm^{-3}, and from these values an *internal* quantum efficiency of 18% is calculated.[14] Measurements of the *external* photoluminescent efficiency on this sample yield ~ 6% when the sample is in air and ~ 10% when the sample is placed in immersion oil to couple more light out. Because of the measurement change with the encapsulating index, one has to use an optical coupling correction to determine the internal efficiency.[39] When this is done, an internal efficiency of 17% is obtained. A small die from the same wafer was separately annealed and a peak efficiency of 17% was obtained in both air and oil; just about all the internally generated light was coupled out. This value is close to that of the maximum observed efficiency.[38]

The reciprocal of the measured minority-carrier lifetime is related to the system parameters by

$$\frac{1}{\tau_L} = N_0\sigma_0 v_{th} + \frac{N_{Zn-O}\sigma_{Zn-O} v_{th}}{1+\tau_t/\tau_{tn}} + \frac{1}{\tau_n}, \qquad (11)$$

where τ_n is the contribution of unidentified centers to the minority-carrier lifetime and the ratio $\tau_t/$

τ_{tn} represents the decreased effectiveness of recombination through the Zn-O complex as measured by the decay time of radiative and Auger processes τ_t, compared to the thermalization time τ_{tn}. The value of τ_t/τ_{tn} at 2×10^{17} cm^{-3} is[14] ~ 5. The fraction of recombination current that flows through the Zn-O complexes at low excitation levels is found to be 0.33 from the time decay data and a set of curves as in Ref. 14 (a value of $\tau_{tn}=200$ nsec is used as obtained from the data of Fig. 8 instead of the 160 nsec value in Ref. 14). Auger processes account for approximately 50% of the recombination,[14] thus resulting in the measured internal quantum efficiency of 17%. Using this fraction of 0.33, the measured minority-carrier lifetime, and the value for the Zn-O complex capture cross section we estimate the complex concentration, $N_{Zn-O} \simeq 4\times10^{15}$ cm^{-3}. This value is lower than those obtained previously from absorption measurements[9,27] with samples which had higher Zn concentrations. A dependence upon Zn concentration is consistent with both absorption studies[40,41] and pairing theory.[4]

Using the Zn-O complex concentration of sample 3 and the annealing conditions (16 h at 600 °C) we derive an oxygen concentration of 7×10^{16} cm^{-3} from Fig. 10. Values in the low 10^{17}-cm^{-3} range were found in Ref. 10 from saturation measurements and concentrations of 7×10^{16} and 2.7×10^{17} cm^{-3}, respectively, in Refs. 11 and 12 from solubility measurements. Utilizing the value of 7×10^{16} cm^{-3} and Eq. (11), the relative fraction of low-level recombination currents through the Zn-O complex, oxygen donor, and unidentified centers are 0.33, 0.37, and 0.3, respectively. The latter two values are subject to the same uncertainties as the oxygen-donor capture cross section and concentration.

Returning to Fig. 3 and Table I we note two other pieces of information; the unannealed sample does not display an increase in red efficiency with excitation, and its minority-carrier lifetime increases by a factor of 3 upon annealing. Both observations support the contention that annealing not only increases the Zn-O complex concentration, but also decreases the contribution of some unidentified center or centers.

A few remarks are made on the saturation data with regard to functional agreement between theory and experiment. In Fig. 3, a theoretical curve is plotted (solid line) for the infrared band using the two-electron oxygen model. The dashed line in Fig. 3 represents saturation behavior assuming the oxygen center is a single-electron center. The functional behavior is similar to that of the red band. The curve can be shifted about by choosing different values for the capture cross section, but under no circumstances does it ap-

proximate the experimental behavior.

A visual comparison of the infrared and red data suggests a correlation between the red efficiency increase and infrared decrease, but sharp saturation of the infrared band at approximately the same intensity as the red band is not consistent with this picture in either the one- or two-electron model of the oxygen center. The data can be better fit if the red superlinearity is assumed associated with saturation of a third center.

C. Unresolved Problems: Radiative Efficiency of Electron on Deep-Electron Oxygen Level

In the previous paragraphs the Zn-O oxygen system has been described along with measurements on a sample which closely approximates this system. A general consistency was observed. However, several problems remain, in particular, with regard to a detailed description of the oxygen donor. The specific problem of the nature and magnitude of nonradiative recombination at the deep level of the oxygen center is an area which we have not previously discussed in this paper. We first cover this topic in some detail, touching upon other unresolved issues in the process, and conclude this section with an enumeration of problems raised in this work.

Bhargava[42] and Dishman[43] have attributed the infrared radiation from the oxygen center above ~ 100 °K to a bound-to-free transition involving a bound electron on the oxygen site and a free hole. This transition contrasts with the donor-acceptor pair band observed at low temperatures.[30] In the work by Dishman et al.[10,43] evidence is presented of a nonradiative component through measurements of both the absolute efficiency at the center[10] and changes in the relative efficiency[43] with temperature. If the nonradiative recombination occurs through an Auger process then its rate is expected to be proportional to some quadratic combination of the free hole and/or neutral acceptor concentrations. Bhargava[42] monitored the time decay τ_0 over a range of free hole concentrations extending over an order of magnitude, observed a linear dependence, and concluded that the nonradiative recombination is not important. We observe a similar dependence (see Table I), although there is some deviation.

Our observations of the excitation-intensity data do not clarify the situation because of the complication of nonradiative processes involving the second bound electron. Furthermore, it is not clear to what extent these processes influenced the conclusions of the earlier workers; there is a finite probability that the below band gap excitation of[10,43] 6328-Å excited the second bound-electron state as well as the first.

Some knowledge of the nonradiative strength can be obtained by monitoring the low-excitation-intensity ratio of the infrared-to-red luminescence. An expression is derived for this ratio from the low-level limits of Eqs. (3) and (8):

$$\frac{L_{ir}}{L_{red}} = \frac{N_0^e/\tau_{0R}}{N_{Zn-O}^e/\tau_R} = \frac{\sigma_0 N_0}{\sigma_{Zn-O} N_{Zn-O}} \frac{\tau_R}{\tau_t'} \frac{\tau_0}{\tau_{0R}} . \quad (12)$$

The parameters τ_{0R} and τ_R represent the radiative times of the oxygen and Zn-O centers, respectively. The ratio τ_R/τ_t' is known[14] and to a good approximation equals 10 over the carrier concentration range of interest. Since the quantity $(\sigma_0 N_0/\sigma_{Zn-O} N_{Zn-O})$ is derived with reasonable accuracy (the product of the capture cross section and concentration is subject to less error than the evaluation of these quantities individually), the spectral evaluation of L_{ir}/L_{red} leads to an estimate of the quantity τ_0/τ_{0R}, and hence the nonradiative component. Spectral measurements on the sample in Fig. 3 give $L_{ir}/L_{red} \simeq 0.3$ which indicates a value for $\tau_0/\tau_{0R} \simeq 0.1$, in agreement with Dishman's conclusions. The oxygen concentration of 7×10^{16} cm^{-3} used in this calculation was obtained from pairing theory.[4] Oxygen concentrations have been reported ranging from 10^{16}–3×10^{17} cm^{-3}. (The fact that this range of concentrations was assembled over many different samples is not as significant as it appears at first sight, since it is believed[13] that the solubility limit was reached in all cases.)

Recently, Kukimoto et al.[44] have measured a substitutional oxygen concentration of 3.0×10^{16} cm^{-3} in a GaP: Zn, O-doped diode using photocapacitive techniques. If their value is substituted into Eq. (12), a value of $\tau_0/\tau_{0R} \sim 1$ is found, in agreement with Bhargava's conclusions.[42] The differences are yet to be reconciled.

We conclude this section with a statement of several problems raised in this paper which require additional work.

(i) An evaluation of the depth of the oxygen center at elevated temperatures (450–600 °K) would clarify the apparent discrepancy between the oxygen-donor deep-electron-capture cross section as determined through excitation-intensity measurements and thermalization measurements.

(ii) Strong confirmation of the validity of two-electron recombination at the oxygen site would be obtained through observation of a radiative band associated with two-electron recombination. One such band would be in the red portion of the spectrum and would be difficult to observe because of interference from competing bands. A second band is expected at energies ≤ 0.9 eV, the result of recombination of a deep electron and the simultaneous ejection of the second electron into the

conduction band. This radiation increases quadratically with excitation intensity at low levels.

(iii) The different behavior of annealed and unannealed samples provides clues to the existence of nonradiative centers which can be annealed out.

VI. CONCLUSION

Luminescent-intensity versus excitation-intensity measurements have been performed on the oxygen-related infrared band in a series of (Zn, O)-doped GaP crystals and in a (Cd, O) and a carbon-doped GaP crystal. We attribute the characteristic sublinear increase of the infrared band over several decades of excitation to recombination involving two electrons at the oxygen site. The energy level of the second electron is deduced from measured quantities to be ≥ 400 meV below the conduction band. The capture cross section of the deep electron is derived from these experiments and from luminescent time-decay measurements on the infrared band in the range 300–600 °K. From these measurements a value of $\sigma_0 \sim 10^{-17} \times (p/10^{17})$ cm^2 is assigned.

Similar measurements were performed on the Zn-O red band with a resultant value of $\sigma_{Zn-O} = 2 \times 10^{-15}$ cm^2. On the basis of these two capture cross sections and previous work,[14] contours were given for the internal Zn-O red-band quantum efficiency as a function of N_{Zn-O}/N_O. A maximum internal quantum efficiency of $\sim 35\%$ is calculated for samples annealed at 600 °C. This upper limit was obtained by setting the maximum value of N_{Zn-O}/N_O according to pairing calculations.[4] A value in the 40% range is predicted if equilibrium pairing is achieved at 500 °C.

The derived model is consistent with measurements on samples that approach the conditions of Zn-O and oxygen as the major recombination centers. The results are also consistent with the long minority-carrier lifetimes, ~ 150 nsec, observed in p-type green-emitting material in which efforts were taken to suppress the oxygen concentration.[18,23]

Several problem areas were reviewed. We conclude by noting the corroboration of the two-electron oxygen model by recent photocapacitance measurements of Kukimoto et al.[44]

[1]T. N. Morgan, B. Welber, and R. N. Bhargava, Phys. Rev. **166**, 751 (1968).

[2]C. H. Henry, P. J. Dean, and J. D. Cuthbert, Phys. Rev. **166**, 754 (1968).

[3]A. Onton and M. R. Lorenz, Appl. Phys. Letters **12**, 115 (1968).

[4]J. D. Wiley, J. Phys. Chem. Solids **32**, 2053 (1971).

[5]J. S. Jayson, following paper, Phys. Rev. B **6**, 2372 (1972).

[6]D. F. Nelson, Phys. Rev. **149**, 574 (1966).

[7]W. Rosenzweig, W. H. Hackett, Jr., and J. S. Jayson, J. Appl. Phys. **40**, 4477 (1969).

[8]J. S. Jayson, J. Appl. Phys. **41** (1970).

[9]A. Kasami, Japan J. Appl. Phys. **9**, 946 (1970).

[10]J. M. Dishman, M. DiDomenico, Jr., and R. Caruso, Phys. Rev. B **2**, 1988 (1970).

[11]L. M. Foster and J. Scardefield, J. Electrochem. Soc. **116**, 494 (1969).

[12]R. H. Saul and W. H. Hackett, Jr., J. Electrochem. Soc. **117**, 921 (1970).

[13]E. C. Lightowlers, J. C. North, A. S. Jordan, L. Derick, and J. L. Merz (unpublished).

[14]J. S. Jayson, R. N. Bhargava, and R. W. Dixon, J. Appl. Phys. **41**, 4972 (1970).

[15]R. Z. Bachrach, Rev. Sci. Instr. **43**, 734 (1972).

[16]W. R. Bennett, Jr., P. J. Kindleman, and G. N. Mercer, Appl. Opt. Suppl. **2**, 35 (1965).

[17]N. E. Schumaker (unpublished).

[18]R. Z. Bachrach, O. G. Lorimor, L. R. Dawson, and K. B. Wolfstirn, Bull. Am. Phys. Soc. **16**, 436 (1971).

[19]P. J. Dean and M. Ilegems (unpublished).

[20]M. Gershenzon and R. M. Mikulyak, Appl. Phys. Letters **8**, 245 (1966).

[21]B. Welber and T. N. Morgan, Phys. Rev. **170**, 767 (1968).

[22]J. S. Jayson and R. Z. Bachrach, Phys. Rev. B **4**, 477 (1971).

[23]R. Z. Bachrach and O. G. Lorimor, J. Appl. Phys. **43**, 500 (1972).

[24]J. S. Jayson and R. W. Dixon, J. Appl. Phys. **42**, 774 (1971).

[25]W. H. Hackett, Jr., J. Appl. Phys. **42**, 3249 (1971).

[26]J. A. W. van der Does de Bye and A. T. Vink, J. Luminescence (to be published).

[27]J. D. Cuthbert, C. H. Henry, and P. J. Dean, Phys. Rev. **170**, 739 (1968).

[28]A. Onton, Phys. Rev. **186**, 786 (1969).

[29]H. C. Casey and J. S. Jayson, J. Appl. Phys. **42**, 2774 (1971).

[30]P. J. Dean and C. H. Henry, Phys. Rev. **176**, 928 (1968).

[31]P. J. Dean, C. H. Henry, and C. J. Frosch, Phys. Rev. **168**, 812 (1968).

[32]M. B. Panish and H. C. Casey, Jr., J. Appl. Phys. **40**, 163 (1969).

[33]R. N. Bhargava, J. Appl. Phys. **41**, 3698 (1970).

[34]J. J. Hopfield, Proceedings of the International Conference on the Physics of Semiconductors, Paris, 1964 (Dunod, Paris, 1964), p. 725.

[35]D. F. Nelson, J. D. Cuthbert, P. J. Dean, and D. G. Thomas, Phys. Rev. Letters **17**, 1262 (1966).

[36]P. J. Dean, Phys. Rev. **157**, 655 (1967).

[37]I. Ladany, J. Electrochem. Soc. **116**, 993 (1969).

[38]K. Maeda, M. Naito, and A. Kasami [Japan J. Appl. Phys. 8, 817 (1969)] have reported a value of 22% in material thinned down to 50 μ. Both N. E. Schumaker and R. H. Saul (unpublished) have measured values of 15–18% on several samples placed in immersion oil to improve the optical coupling efficiency. From the reported data in the former reference and data in media other than oil in the latter work a peak internal efficiency of ~ 25% is obtained.

[39]W. B. Joyce, R. Z. Bachrach, R. W. Dixon, D. A. Sealer (unpublished).
[40]S. D. Lacey, Solid State Commun. 8, 1115 (1970).
[41]J. M. Dishman and M. DiDomenico, Jr., Phys. Rev. B 4, 2621 (1971).
[42]R. N. Bhargava, Phys. Rev. B 2, 387 (1970).
[43]J. M. Dishman, Phys. Rev. B 3, 2588 (1971).
[44]H. Kukimoto, C. H. Henry, and G. L. Miller, Appl. Phys. Letters (to be published).

Analysis of Recombination of Excitons Bound to Deep Neutral Donors and Acceptors

J. S. Jayson

Bell Telephone Laboratories, Incorporated, Murray Hill, New Jersey 07974

(Received 23 March 1972)

On the basis of the plausibility arguments and experimental results of previous workers on shallow-donor and -acceptor levels, the recombination of bound excitons at deep-neutral-donor and -acceptor sites via an Auger process appears to be a likely candidate for a nonradiative or "killer" mechanism in luminescent material. We analytically investigate the effects of this center in a p-type semiconductor (the results can be extended in a straightforward manner to n-type material) with the goal of uncovering experimentally verifiable properties. The analysis specializes in several specific examples. The first case is that in which the competing nonradiative-recombination mechanism is a shallow exciton bound to an acceptor. For this case the strength of the nonradiative recombination goes through a maximum as a function of temperature, and this effect would be experimentally observed as a minimum in the radiative efficiency of the semiconductor. Such an effect is reported in GaP(Zn, O) in an accompanying paper. Furthermore, on the basis of numerical calculations presented in this paper we consider it unlikely that the silicon acceptor, which has been suggested as a possible nonradiative center in GaP, is a strong recombination site. The second example considered is that of an exciton bound to a neutral donor. Since this situation involves capture of two minority carriers by the donor, the concentrations of the captured electrons are expected to depend nonlinearly on excitation intensity. These effects are easily observed if electrons in either state give rise to a detectable radiative band. In the accompanying paper the intensity variation of the oxygen-donor infrared band in GaP(Zn, O) with excitation level is interpreted in terms of the above model. An approximate time-dependent solution is obtained for the deep-level population which yields an initial fast decay at high-excitation levels. This fast component, which is due to two-electron-recombination processes, has also been observed in the GaP oxygen-donor infrared band.

I. INTRODUCTION

There is abundant theoretical[1] and experimental[2-7] evidence demonstrating the existence and stability of hole and electron pairs bound as excitons to neutral donors and acceptors. Because there are three bound particles present in this configuration, nonradiative recombination through an Auger process is highly probable and, in fact, is observed to be orders of magnitude greater than the accompanying radiative recombination.[4,6,7] (The low radiative efficiency of these centers contrasts with the high efficiencies obtained from excitons bound to isoelectronic centers, for example, nitrogen[8] and the zinc-oxygen nearest-neighbor complex[9,10] in GaP, where only two particles are bound, thus precluding the possibility of an intrinsic Auger process.) It has furthermore been suggested that

the Auger process would render *deep* donors or acceptors particularly effective as nonradiative centers because of the large overlap of the bound-particle wave functions.[7] In this paper we analyze the recombination kinetics associated with such deep sites and attempt to identify experimentally verifiable clues which can be utilized to uncover these usually unwanted centers. Some experimental evidence of these effects has recently been observed for the oxygen donor in GaP, and these results are presented in an accompanying paper.[11]

II. ANALYSIS

For clarity the analysis will be specialized to p-type material, but the results can be carried over to n-type material in a straightforward manner. Deep centers are expected to be of most interest, but the activation energy of the first bound